Journal of Nuclear Materials 401 (2010) 13–16

Contents lists available at ScienceDirect

Journal of Nuclear Materials

journal homepage: www.elsevier.com/locate/jnucmat

Precipitation of ferromagnetic phase induced by defect energies during creep deformation in Type 304 austenitic steel

Yuhki Tsukada [a,*], Atsuhiro Shiraki [a,1], Yoshinori Murata [a], Shigeru Takaya [b], Toshiyuki Koyama [c], Masahiko Morinaga [a]

[a] Department of Materials, Physics and Energy Engineering, Graduate School of Engineering, Nagoya University, Furo-cho, Chikusa-ku, Nagoya 464-8603, Japan
[b] Japan Atomic Energy Agency, 4002 Narita-cho, O-arai-machi, Higashi-ibaraki-gun, Ibaraki 311-1393, Japan
[c] National Institute for Materials Science, 1-2-1 Sengen, Tsukuba, Ibaraki 305-0047, Japan

ARTICLE INFO

Article history:
Received 16 December 2009
Accepted 17 March 2010

ABSTRACT

The correlation of defect energies with precipitation of the ferromagnetic phase near $M_{23}C_6$ carbide during creep tests at high temperature in Type 304 austenitic steel was examined by estimating the defect energies near the carbide, based on micromechanics. As one of the defect energies, the precipitation energy was calculated by assuming $M_{23}C_6$ carbide to be a spherical inclusion. The other defect energy, creep dislocation energy, was calculated based on dislocation density data obtained from transmission electron microscopy observations of the creep samples. The dislocation energy density was much higher than the precipitation energy density in the initial stage of the creep process, when the ferromagnetic phase started to increase. Creep dislocation energy could be the main driving force for precipitation of the ferromagnetic phase.

1. Introduction

Type 304 austenitic steel is a high temperature material that is applied in structural components of nuclear power plants. Though it exhibits paramagnetism at room temperature as a metastable state, it was reported that its magnetic properties changed during creep tests at high temperature, and magnetization was detected. This phenomenon has not been observed in the grip (stress free) portion. It has been confirmed that the change in magnetic properties in the gauge portion originates from transformation from the fcc phase to the bcc phase, which is particularly observed near $M_{23}C_6$ carbides [1,2]. The region near the carbide is known as a stress concentration zone, where cavity formation has been observed in the late stage of the creep process; hence, it has been proposed that the formation of the ferromagnetic phase is related to creep damage. The amount of the ferromagnetic phase starts to increase before cavities are observed [2]; therefore, it is useful to correlate the magnetization with creep damage, since there is a possibility of developing a non-destructive evaluation technique in which creep damage can be estimated by detecting changes in the magnetic properties.

For understanding the formation mechanism of the ferromagnetic phase in Type 304 steel, it is necessary to examine the defect energies in the material; the distribution of defect energies affects the total free energy change associated with the formation of nuclei and makes certain locations preferred nucleation sites [3,4]. In the creep process in Type 304 steel, there are two types of defect energy in the region near the $M_{23}C_6$ carbide: elastic strain energy originating from the precipitation of the carbide (precipitation energy), and elastic strain energy from creep dislocations trapped by carbides during the creep process (dislocation energy). Both of these defect energies can be expressed in a form as energy per unit volume, and can be incorporated into the typical driving force for nucleation of the ferromagnetic phase in the classical nucleation theory.

The purpose of this study is to examine the correlation of the defect energies with the precipitation of the ferromagnetic phase during the creep process. Defect energies near $M_{23}C_6$ carbide are estimated based on micromechanics [5], and dislocation density near the carbide, essential for calculating the dislocation energy, is measured from transmission electron microscopy (TEM) observations of creep samples. The formation mechanism of the ferromagnetic phase is discussed considering both the equilibrium phase stability of the material and the estimated defect energy densities.

2. Experimental procedures

The chemical composition of the Type 304 austenitic steel used in this study is listed in Table 1. Specimens with a gauge diameter of 10 mm and gauge length of 50 mm were prepared. Creep

* Corresponding author. Tel.: +81 52 789 5342; fax: +81 52 789 3232.
E-mail address: tsukada@silky.numse.nagoya-u.ac.jp (Y. Tsukada).
[1] Present address: Kobe Steel, Ltd., 2222-1 Onoecho Ikeda, Kakogawa, Hyogo 675-0023, Japan.

0022-3115/$ - see front matter © 2010 Elsevier B.V. All rights reserved.
doi:10.1016/j.jnucmat.2010.03.013

Table 1
Chemical composition of Type 304 steel used in this study.

Element	C	Si	Mn	Ni	Cr	Fe
Mass%	0.05	0.60	0.87	8.94	18.59	Bal.

rupture and creep interrupt tests were carried out at 873 K under 172 MPa, in air.

Extraction residue analysis was performed to determine the amount of $M_{23}C_6$ carbide precipitating during the creep test. The carbides were quantitatively extracted by potentiostatic electrolysis in 10%AA–1%TMAC–methanol electrolyte [6].

Thin foils were prepared from the interrupted creep samples for TEM observation with a twin-jet electropolisher, using a solution of 10% perchloric acid and 90% ethanol at 233 K. Dislocation density in the material was measured by intersection analysis from TEM micrographs as

$$\rho = \frac{2N}{L\delta}, \tag{1}$$

where N is the intersection number of dislocations in a line with a length of L, and δ is the foil thickness [7]. In this study, $M_{23}C_6$ carbide was regarded as a spherical inclusion (Ω), and the dislocation density in the matrix near the carbide was measured in the region between the spherical $M_{23}C_6$ carbide with radius of R and the sphere with radius of $(R + l)$, as indicated by the shadowed area in Fig. 1, where l is the distance from the interface between the carbide and the matrix.

3. Calculation method

3.1. Dislocation energy near the $M_{23}C_6$ carbide

The dislocation energy density near the $M_{23}C_6$ carbide was evaluated by:

$$E_d = \left[\frac{\mu b^2}{4\pi}\ln\left(\frac{r}{r_0}\right)\right]\cdot\rho, \tag{2}$$

where μ is the shear modulus, b is the magnitude of the Burgers vector, r_0 is the cutoff radius of the dislocation core, r is the outer cutoff radius, and ρ is the dislocation density. In this study, r_0 and r are set to $r_0 = 5b$ and $r = b \times 10^4$, and experimentally obtained data on the dislocation density near the carbide were used in this calculation. Theoretically, the term $(\mu b^2/4\pi)\cdot\ln(r/r_0)$ in Eq. (2) is the elastic strain energy of a straight screw dislocation per unit length in an infinite body [8], but in this study, the local dislocation energy density in the region where a large number of dislocations occur with complicated configurations was approximated based on Eq. (2).

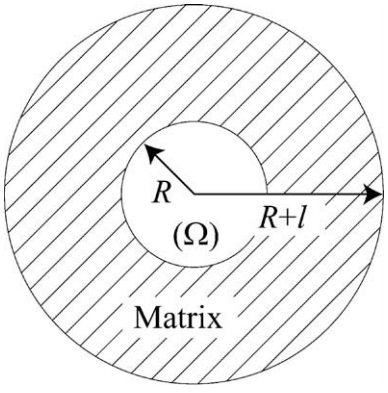

Fig. 1. Schematic illustration of matrix region between a spherical inclusion (Ω) with radius of R and a sphere with radius of $(R + l)$, where l is the distance from the interface between the inclusion and the matrix.

3.2. Precipitation energy of $M_{23}C_6$ carbide

Precipitation energy of $M_{23}C_6$ carbide is evaluated based on micromechanics [5]. The Green's function for elastically isotropic and homogeneous inclusion with shear modulus μ and Poisson's ratio ν is given by

$$G_{km}(\mathbf{x}-\mathbf{x}') = \frac{\bar{x}_k\bar{x}_m/\bar{x}^3 + (3-4\nu)\delta_{km}/\bar{x}}{16\pi(1-\nu)\mu}, \tag{3}$$

where $\bar{x}_k = x_k - x'_k$, $\bar{x} = (\bar{x}_k\bar{x}_k)^{1/2}$, and δ_{ij} is the Kronecker delta function. The displacement $u_k(\mathbf{x})$ at position $\mathbf{x}$ in the material containing the inclusion Ω with uniform eigenstrain ε^0_{mn} is given by

$$u_k(\mathbf{x}) = -\int_\Omega C_{pqmn}\varepsilon^0_{mn}\frac{\partial G_{pk}(\mathbf{x}-\mathbf{x}')}{\partial x_q}d\mathbf{x}', \tag{4}$$

where $C_{ijkl} = [2\mu\nu/(1-2\nu)]\delta_{ij}\delta_{kl} + \mu(\delta_{ik}\delta_{jl} + \delta_{il}\delta_{jk})$ are the elastic constants of the material. The eigenstrain ε^0_{mn} is defined as

$$\varepsilon^0_{mn} = \delta_{mn}\varepsilon_0 s(\mathbf{x}), \tag{5}$$

where ε_0 is the pure dilatation coefficient, and $s(\mathbf{x})$ is step function which equals 1 within Ω and 0 outside Ω. When Ω is a spherical inclusion with radius R, the total strain outside Ω is calculated as

$$\begin{aligned}\varepsilon_{kl}(\mathbf{x}) &= \tfrac{1}{2}\left(\tfrac{\partial u_k(\mathbf{x})}{\partial x_l} + \tfrac{\partial u_l(\mathbf{x})}{\partial x_k}\right)\\ &= -\tfrac{1}{2}\int_\Omega C_{pqmn}\varepsilon^0_{mn}\left(\tfrac{\partial^2 G_{pk}(\mathbf{x}-\mathbf{x}')}{\partial x_l\partial x_q} + \tfrac{\partial^2 G_{pl}(\mathbf{x}-\mathbf{x}')}{\partial x_k\partial x_q}\right)d\mathbf{x}'\\ &= \tfrac{1+\nu}{3(1-\nu)}\varepsilon_0 R^3\left(\tfrac{\delta_{kl}}{x^3} - 3\tfrac{x_k x_l}{x^5}\right),\end{aligned} \tag{6}$$

where $x = \sqrt{x_i x_i}$. Accordingly, the local precipitation energy density outside Ω can be calculated as

$$\begin{aligned}E_p(\mathbf{x}) &= \tfrac{1}{2}C_{ijkl}\varepsilon_{ij}(\mathbf{x})\varepsilon_{kl}(\mathbf{x})\\ &= \tfrac{2\mu(1+\nu)^2}{3(1-\nu)^2}\varepsilon_0^2\tfrac{R^6}{x^6}.\end{aligned} \tag{7}$$

From Eq. (7), averaged precipitation energy density $\bar{E}_p$ in the shadowed area in Fig. 1 was calculated as

$$\bar{E}_p = \frac{2\mu(1+\nu)^2}{3(1-\nu)^2}\varepsilon_0^2 R^6\left[\frac{1}{R^3} - \frac{1}{(R+l)^3}\right]\cdot\left[\frac{1}{(R+l)^3 - R^3}\right]. \tag{8}$$

4. Results

4.1. Change in mole fraction of $M_{23}C_6$ carbide

The results of extraction residue analysis are summarized in Fig. 2, which shows the change in the mole fraction of $M_{23}C_6$

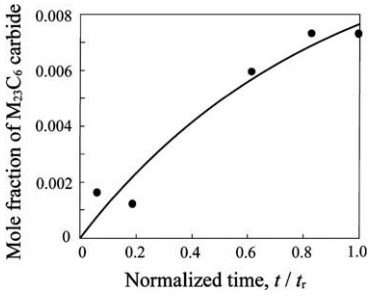

Fig. 2. Change in mole fraction of $M_{23}C_6$ carbide with creep time normalized by rupture time (t_r).

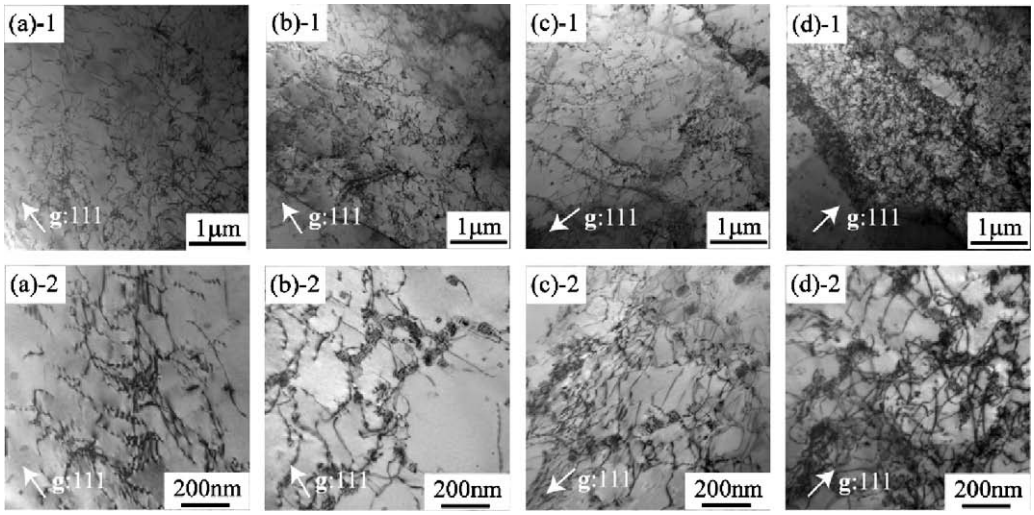

Fig. 3. TEM micrographs of creep samples: (a) $t/t_r = 0.186$, (b) $t/t_r = 0.614$, (c) $t/t_r = 0.830$ and (d) $t/t_r = 1$ where t_r is rupture time ($\mathbf{g}: 1\,1\,1$, $\mathbf{B}: [0\,\bar{1}\,1]$).

carbide with the creep time normalized by the rupture time t_r ($t_r = 780$ h). Information on the mass fraction of the carbide obtained from the extraction residue analysis was transformed to a mole fraction using the molar mass of 54.89 g/mol for Type 304 steel and 44.04 g/mol for $M_{23}C_6$ carbide. The amount of carbide increases with the creep time, and reaches a mole fraction of 0.0073 at $t/t_r = 1$.

4.2. Dislocation energy density near the $M_{23}C_6$ carbide

Fig. 3 shows TEM micrographs taken from the creep samples. In Fig. 3, the results for four different creep times are shown: (a) $t/t_r = 0.186$, (b) $t/t_r = 0.614$, (c) $t/t_r = 0.830$ and (d) $t/t_r = 1$, where t_r is the rupture time. From Fig. 3, it is shown that the creep dislocations are trapped by finely precipitated carbides. The carbides are about 9 nm in radius at $t/t_r = 0.186$ and coarsen to about 23 nm in radius at $t/t_r = 1$. Furthermore, it is obvious that the dislocation density near the carbides increases with the creep time.

From the TEM micrographs, the dislocation energy density E_d was evaluated following Eq. (2) for the shadowed area in Fig. 1, where the distance from the interface of the carbide was set to $l = 50$ or 100 nm. In the calculation, physical parameters of $\mu = 77.4$ GPa [9] and $b = 0.255$ nm [10] were used; the results of E_d are shown in Fig. 4 where the dislocation energy density becomes high when the analytical area decreases from 100 to 50 nm near the carbide; hence, the dislocation energy is found to concentrate near the carbide. There is a tendency for the dislocation energy density to increase with the creep time, although it scarcely changes during $t/t_r = 0.2$–0.6.

4.3. Precipitation energy density of $M_{23}C_6$ carbide

Precipitation energy density of the carbide $\overline{E}_p$ was evaluated following Eq. (8) for the shadowed area in Fig. 1, and the distance from the interface of the carbide was set to $l = 50$ or 100 nm to coincide with the conditions in Section 4.2. The physical parameters in Eq. (8) were set to: $\mu = 77.4$ GPa [9], $\nu = 0.290$ [9], and $\varepsilon_0 = -0.017$ [11]. The calculation results of $\overline{E}_p$ as a function of the radius of the carbide are shown in Fig. 5; smaller the distance to the carbide, higher the precipitation energy density. Furthermore, it is obvious that the precipitation energy density near the carbide increases with the coarsening of the carbide.

5. Discussion

For the steel used in this study, the amount of equilibrium phases, in mole fraction, at 873 K are calculated to be 0.011 for $M_{23}C_6$ carbide, 0.018 for σ phase, 0.335 for bcc (α) phase, and 0.636 for fcc (γ) phase, based on the thermodynamic database

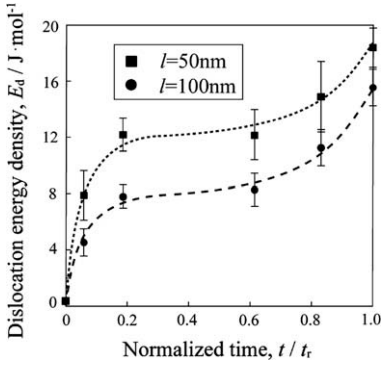

Fig. 4. Change in dislocation energy density in shadowed area in Fig. 1 with creep time normalized by rupture time (t_r). l is the distance from the interface between $M_{23}C_6$ carbide and the matrix.

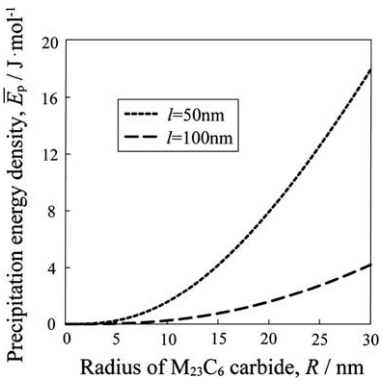

Fig. 5. Precipitation energy density in shadowed area in Fig. 1 as a function of radius of $M_{23}C_6$ carbide. l is the distance from the interface between the carbide and the matrix.

(Thermo-Calc Ver. FE-6). In this study, σ phase was not detected in any samples, and this result is consistent with the time–temperature-precipitation (TTP) diagram reported previously [12].

From the fact that the α phase does exist as an equilibrium phase at 873 K, it can be said that the ferromagnetic α phase would precipitate during the creep process if some defect energies were increasing during creep, as shown in Figs. 4 and 5; this can be the driving force for the precipitation. In fact, these defect energies concentrate near the $M_{23}C_6$ carbide; this makes the nucleation of the α phase near the carbide more frequent event. This result agrees well with the previous report that the ferromagnetic phase is particularly observed near the $M_{23}C_6$ carbides [1,2]. In Fig. 4, the reason that the dislocation energy density is constant for $t/t_r = 0.2$–0.6 seems to be that the introduction of creep dislocation during creep deformation is balanced out with recovery of the dislocation. A previous study reported that the amount of the ferromagnetic phase started to increase around $t/t_r = 0.2$ in a creep test at 923 K under 118 MPa [2]. Fig. 4 shows that the dislocation energy density E_d is 12.2 J/mol when $l = 50$ nm, and 7.8 J/mol when $l = 100$ nm at $t/t_r = 0.186$. On the other hand, from the fact that the carbide is about 9 nm in radius at $t/t_r = 0.186$, the precipitation energy density of the carbide $\overline{E}_p$ is 1.2 J/mol when $l = 50$ nm, and 0.2 J/mol when $l = 100$ nm (Fig. 5). This suggests that the defect energy, which plays a dominant role in the precipitation of the α phase during the creep process, is the dislocation energy near the carbides.

Strictly speaking, the precipitation energy of the carbide should be assessed considering an anisotropic and elastically inhomogeneous body. Furthermore, it has been reported that the carbide takes energetically favorable shapes, such as rectangle, square, or rhomboid, in the coarsening process [11]. Thus, the estimated value of $\overline{E}_p$ in Fig. 5 may not accurately represent the energy in a practical alloy. However, especially when the precipitated carbide is fine, it seems reasonable to assume the carbide is a spherical inclusion; hence, it is certain that the dislocation energy density is significantly greater than the precipitation energy density of the carbide around $t/t_r = 0.2$ in this study.

6. Conclusions

Defect energies near $M_{23}C_6$ carbides during the creep process were evaluated based on micromechanics, and the correlation of defect energies with the formation of the ferromagnetic phase was examined. The precipitation energy density of $M_{23}C_6$ carbide was calculated by considering the carbide as a spherical inclusion, whereas the dislocation energy density was evaluated based on the experimental data on the dislocation density near the carbide. It was shown that the dislocation energy density was significantly higher than the precipitation energy density in the initial stage of the creep process when the ferromagnetic phase started to increase. Thus, dislocation energy plays a dominant role in the precipitation of the ferromagnetic phase in Type 304 austenitic steel.

Acknowledgements

This work was supported by a Grant-in-Aid for JSPS Fellows of the Ministry of Education, Culture, Sports, Science and Technology, Japan, and was also supported in part by a Grant-in-Aid for Scientific Research of Japan Society for the Promotion of Science (JSPS), Japan.

References

[1] Y. Nagae, Mater. Sci. Eng. A 387–389 (2004) 665–669.
[2] Y. Nagae, K. Aoto, J. Soc. Mater. Sci., Japan 54 (2005) 116–121.
[3] C. Shen, J.P. Simmons, Y. Wang, Acta Mater. 54 (2006) 5617–5630.
[4] C. Shen, J.P. Simmons, Y. Wang, Acta Mater. 55 (2007) 1457–1466.
[5] T. Mura, T. Mori, Micromechanics, Baifu-kan, Tokyo, 1976.
[6] H. Kutsumi, A. Chino, Y. Ishibashi, Tetsu-to-Hagané 78 (1992) 594–600.
[7] P.B. Hirsch, A. Howie, R.B. Nicholson, D.W. Pashley, M.J. Whelan, Electron Microscopy of Thin Crystals, Butterworth, London, 1965.
[8] M. Kato, Introduction to the Theory of Dislocations, Shokabo, Tokyo, 1999.
[9] H.M. Ledbetter, J. Appl. Phys. 52 (1981) 1587–1589.
[10] A. Boeuf, S. Crico, R. Caciuffo, F. Rustichelli, I. Pomot, G. Uny, Mater. Lett. 3 (1985) 115–118.
[11] F.R. Beckitt, B.R. Clark, Acta Metall. 15 (1967) 113–129.
[12] H. Tanaka, M. Murata, K. Kamihira, K. Kimura, Report of the 123rd Committee on Heat-Resisting Materials and Alloys, Japan Society for the Promotion of Science, 2008, pp. 277–291.